JACS
JOURNAL OF THE AMERICAN CHEMICAL SOCIETY

Article

pubs.acs.org/JACS

Carborane-Based Optoelectronically Active Organic Molecules: Wide Band Gap Host Materials for Blue Phosphorescence

Kyung-Ryang Wee,[†] Yang-Jin Cho,[†] Soyeong Jeong,[†] Soonnam Kwon,*[,†] Jong-Dae Lee,[‡] Il-Hwan Suh,[†] and Sang Ook Kang*[,†]

[†]Department of Advanced Materials Chemistry, Korea University, 2511 Sejong-ro, Sejong 339-700, South Korea

[‡]Department of Chemistry, Chosun University, Gwangju, South Korea

Supporting Information

ABSTRACT: Carborane-based host materials were prepared to fabricate deep blue phosphorescence organic light-emitting diodes (PHOLEDs), which constituted three distinctive geometrical structures stemming from the corresponding three different isomeric forms of carboranes, namely, *ortho*-, *meta*-, and *para*-carboranes. These materials consist of two carbazolyl phenyl (CzPh) groups as photoactive units on each side of the carborane carbons to be bis[4-(*N*-carbazolyl)phenyl]-carboranes, ***o*-Cb**, ***m*-Cb**, and ***p*-Cb**. To elaborate on the role of the carboranes, comparative analogous benzene series (***o*-Bz**, ***m*-Bz**, and ***p*-Bz**) were prepared, and their photophysical properties were compared to show that advantageous photophysical properties were originated from the carborane structures: high triplet energy. Unlike ***m*-Bz** and ***p*-Bz**, carborane-based ***m*-Cb** and ***p*-Cb** showed an unconjugated nature between two CzPh units, which is essential for the blue phosphorescent materials. Also, the carborane hosts showed high glass transition temperatures (T_g) of 132 and 164 °C for ***m*-Cb** and ***p*-Cb**, respectively. Albeit ***p*-Cb** exhibited slightly lower hole mobility when compared to ***p*-Bz**, it still lies at the high end hole mobility with a value of 1.1×10^{-3} cm^2/(V s) at an electric field of 5×10^5 V/cm. Density functional theory (DFT) calculations revealed that triplet wave functions were effectively confined and mostly located at either side of the carbazolyl units for ***m*-Cb** and ***p*-Cb**. Low-temperature PL spectra indeed provided unequivocal data with higher triplet energy (T_1) of 3.1 eV for both ***m*-Cb** and ***p*-Cb**. ***p*-Cb** was successfully used as a host in deep blue PHOLEDs to provide a high external quantum efficiency of 15.3% and commission internationale de l'elcairage (CIE) coordinates of (0.15, 0.24).

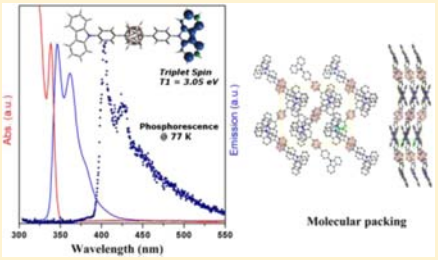

INTRODUCTION

It has been widely accepted that conjugated aromatic compounds containing an aryl basic unit have provided controllable optoelectronic properties essential to organic electronic materials for electroluminescence devices,[1a] organic thin film transistors,[1b] and solar cells.[1c] Given the wide spectrum of advantageous optoelectronic properties made out of the aryl structural motif, there is still a lack of desirable material specifications for high performance device applications, particularly in the deep blue phosphorescent organic light-emitting diodes (PHOLEDs). Most of all, the wide energy gap is the most demanding material property in the development of deep blue PHOLEDs.[2] For example, several approaches have been developed in regards to wide band gap materials for blue phosphorescence. One of the strategies is to use the meta-positions of benzene as the substitution sites, keeping the property of organic functional groups abreast of their own, not altered by benzene resonance.[3,4] However, this method only allowed maximum triplet energy (T_1) of 2.75 eV due to incomplete triplet wave function confinement on either side of the functional unit. Another method is to utilize the silicon atom as a conjugation breaker in between the organic functional groups; it turns out to be the most effective to confine triplet wave function into the organic functional group because the silicon atom is larger than the carbon atom and, hence, it effectively mismatches the electronic π-type overlaps in the surrounding electro-active organic functional groups.[5] However, for the practical application to the vacuum deposition process, further molecular architecture would be required; it must bear higher glass transition temperature (T_g) yet allow reasonable volatility. It is expected that to achieve good thermal property more functional units should be attached to the silicon atom to increase molecular weight, but this opposes the specification for sufficient volatility regarding vacuum evaporation. So, there still remains a challenge to develop an efficient method from which higher triplet energy can be achieved maintaining high T_g and at the same time allowing appropriate volatility.

Taking a lesson from the successful concept of the silicon π-conjugation breaker, we then extend this strategy to cluster carborane in hopes that carborane can function not only as a conjugation breaker but also as an auxiliary for high T_g. Carboranes are known as inorganic analogues of benzene,[6] in which two carbon and ten boron atoms constitute a 12 vertex icosahedral structure and three different geometrical isomers are formed depending on the two carbon atomic positions. Due to the electron sharing nature of the cluster bonding found in

Received: July 9, 2012
Published: October 11, 2012

   dx.doi.org/10.1021/ja3066623 | *J. Am. Chem. Soc.* 2012, 134, 17982−17990

carboranes, they are often regarded as electron-withdrawing and thermally stable functional units. On the basis of these perceptions, several organic or polymeric materials funtionalized by carboranes have been prepared, and advantageous physical properties such as thermal and oxidative stabilities were reported.[7] However, any systematic attempt to unveil the true nature of carborane for organic electronic materials has never been made before in comparison to benzene.

Recently, we elaborated on the unique photophysical properties of *ortho*-carborane, when it was functionalized by an opto-electronically active substituent, carbazolyl phenyl (CzPh).[8a] It was noted that *ortho*-carborane showed enhanced charge transfer (CT) emission due to the electron-deficient character of the carborane coupled to juxtaposition of Ph groups attached to the carbon atoms in the cage.[8] On the contrary, the other isomers did not show CT emission. In this study, we explore the potential utility of carboranes as active structural elements for use in optoelectronic materials. To unveil carboranes' contribution to physical properties in optoelectronic materials clearly, iso-structural benzene analogues are referenced together.

As can be seen in Chart 1, both benzene and carborane cores can be functionalized by carbazolyl phenyl (CzPh) units with a

Chart 1. Three Different Geometrical Isomers Functionalized by CzPhs at Either the Carborane or Benzene Framework

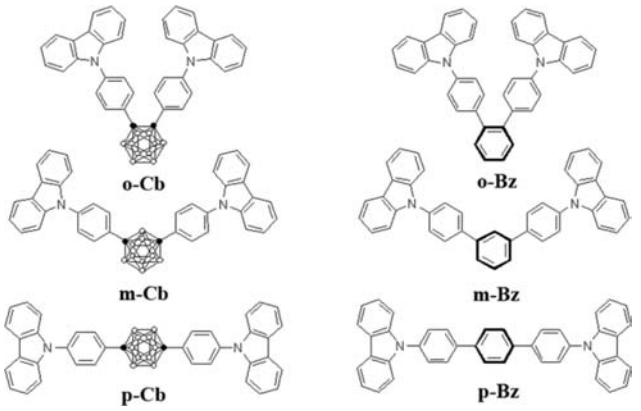

desire of developing potential blue host materials. The resultant two sets of the corresponding three isomeric structures comprising ortho-, meta-, and para-substitutions are clearly seen: The alias for each of those are named to be ***o*-Bz**, ***m*-Bz**, and ***p*-Bz** and ***o*-Cb**, ***m*-Cb**, and ***p*-Cb** for the benzene system and carborane system, respectively.

The physical properties, including photophysical properties, electronic structure, charge mobility, and thermal properties, have been thoroughly investigated for those six compounds. Then, deep blue PHOLEDs were fabricated using the carborane-based materials as hosts in the emission layer (EML) to examine the feasibility for application to OLEDs, in which ***p*-Cb** exhibited excellent device results. Thus, we offer a novel synthetic strategy of using para-linked carborane as an active structural element of material owing to its outstanding advantages: high triplet energy, high charge mobility, and formation of glass film with high thermal stability.

EXPERIMENTAL SECTION

General Procedures. All reactions were carried out in a dry N_2 atmosphere. Solvents were distilled from calcium hydride for dichloromethane (CH_2Cl_2), acetonitrile (CH_3CN), and dimethylformamide (DMF) or from sodium/benzophenone for tetrahydrofuran (THF), ethylene glycol dimethylether (DME), and toluene under a nitrogen atmosphere and stored over molecular sieves. Other reagents were obtained commercially and used without further purification. Glassware, syringes, magnetic stirring bars, and needles were dried in a convection oven for >4 h. Reactions were monitored with thin layer chromatography (TLC). Commercial TLC plates (Merck Co.) were developed, and the spots were identified under UV light at 254 and 365 nm. Column chromatography was done on silica gel 60 G (particle size 5−40 μm, Merck Co.). All synthesized compounds were characterized by ^{1}H NMR, ^{13}C NMR, and HRMS (FAB) mass analysis. The ^{1}H and ^{13}C NMR spectra were recorded on a Varian Mercury 300 spectrometer operating at 300.1 and 75.4 MHz, respectively. The elemental analyses (Carlo Erba Instruments CHNS-O EA 1108 analyzer) and high-resolution tandem mass spectrometry (Jeol LTD JMS-HX 110/110A) were performed by the Ochang branch of the Korean Basic Science Institute. All reagents were purchased and used as received. 9-(4-Bromophenyl)carbazole[9] and 4-(carbazol-9-yl) phenylboronic acid[10] were prepared using the methods reported in the literature.

9,9′-(1,1′:2′,1″-Terphenyl-4,4″-diyl)dicarbazole (*o*-Bz). 1,2-Dibromobenzene (0.25 mL, 2.06 mmol), 4-(carbazol-9-yl)-phenylboronic acid (1.3 g, 4.53 mmol), $Pd(PPh_3)_4$ (0.095 g, 4 mol %), and K_2CO_3 (1.875 g, 29.9 mmol) were charged to a flask. Then toluene/H_2O (33/11 mL) was added to the flask, and the resulting mixture was stirred under N_2 at 110 °C overnight. The organic layer was extracted with CH_2Cl_2 (3 × 30 mL) and dried over magnesium sulfate. The solvent was removed under reduced pressure, and the residue was purified by silica gel column chromatography using CH_2Cl_2/hexane (1:6) as the eluent. ***o*-Bz** was obtained as a white powder (0.78 g, 68%) and further purified by train sublimation in a 62% yield. ^{1}H NMR ($CDCl_3$): δ 8.15 (d, 4H), 7.62 (d, 4H), 7.54−7.42 (m, 8H), 7.42−7.33 (m, 8H), 7.26 (t, 4H). ^{13}C NMR ($CDCl_3$): δ 140.8, 140.6, 140.0, 136.3, 131.5, 130.6, 128.1, 126.6, 126.1, 123.4, 120.4, 120.0, 109.7. HRMS(FAB) calcd for $C_{42}H_{28}N_2$: 560.2252. Found: 560.2201 $[M]^+$. Anal. Calcd for $C_{42}H_{28}N_2$: C, 89.97; H, 5.03; N, 5.00. Found: C, 89.93; H, 5.05; N, 4.97.

9,9′-(1,1′:3′,1″-Terphenyl-4,4″-diyl)dicarbazole (*m*-Bz). A procedure analogous to that used for the synthesis of ***o*-Bz** was used, but starting from 1,3-dibromobenzene (0.25 mL, 2.06 mmol) instead. ***m*-Bz** was obtained as a white powder (0.81 g, 70%) and further purified by train sublimation in a 72% yield. ^{1}H NMR ($CDCl_3$): δ 8.18 (d, 4H), 8.01 (s, 1H), 7.93 (d, 4H), 7.77−7.60 (m, 7H), 7.53−7.42 (m, 8H), 7.29 (t, 4H). ^{13}C NMR ($CDCl_3$): δ 141.1, 140.9, 140.1, 137.2, 128.8, 127.5, 126.5, 126.2, 126.1, 123.5, 120.5, 120.1, 109.9. HRMS(FAB) calcd for $C_{42}H_{28}N_2$: 560.2252. Found: 560.2292 $[M]^+$. Anal. Calcd for $C_{42}H_{28}N_2$: C, 89.97; H, 5.03; N, 5.00. Found: C, 89.99; H, 4.98; N, 4.96.

Crystal Structure Determination. Crystals of ***p*-Cb** and ***p*-Bz** were obtained in a CH_2Cl_2/toluene solution, sealed in glass capillaries under argon, and mounted on the diffractometer. The preliminary examination and data collection were performed using a Bruker SMART CCD detector system single-crystal X-ray diffractometer equipped with a sealed-tube X-ray source (50 kV × 30 mA) using graphite-monochromated Mo Kα radiation (λ = 0.71073 Å). The preliminary unit cell constants were determined using a set of 45 narrow-frame (0.3° in ω) scans. To exclude noise, the double pass method of scanning was used to exclude noise. The collected frames were integrated using an orientation matrix determined from the narrow-frame scans. The SMART software package was used for data collection, and SAINT was used for frame integration.[11] The final cell constants were determined through global refinement of the *xyz* centroids of the reflections harvested from the entire data set. Structure solution and refinement were carried out using the SHELXTL-PLUS software package.[12]

dx.doi.org/10.1021/ja3066623 | J. Am. Chem. Soc. 2012, 134, 17982−17990

Absorption, Fluorescence, and Phosphorescence. The absorption and photoluminescence spectra were recorded on a Shimadzu UV-3101PC UV−vis−NIR scanning spectrophotometer and a Varian Cary Eclipse fluorescence spectrophotometer, respectively. The triplet energies were taken as the maximum of the first vibronic transition regarding the phosphorescence spectra. The samples dissolved in 2-methyl tetrahydrofuran (MTHF) were frozen in liquid nitrogen to 77 K. Phosphorescence was observed by irradiation of the samples at 309 nm using the third harmonic of a Q-switched Nd:YAG laser (Continuum, Surelite II, pulse width of 4.5 ns) combined with a homemade Raman shifter. Temporal profiles were measured by a photomultiplier (Zolix Instruments Co., CR 131) and a digital oscilloscope (Tektronix, TDS-784D) equipped with a monochromator (DongWooOptron, Monora 500i). Reported signals were obtained as averages of 500 events. The detection window was set to 15 μs, and the delay was set to 1 ms from the rigging edge of the laser.

Thermal Property. Thermal property was measured using differential scanning calorimetry (Perkin-Elmer/Pyris Diamond DSC). A heating rate of 10 °C/min was used after first melting the compound, followed by a rapid cooling rate of 40 °C/min to room temperature.

Cyclic Voltammetry (CV). Cyclic voltammetry experiments were performed using a BAS 100 electrochemical analyzer. A three-electrode cell system was used with a glassy carbon, platinum wire, and $Ag/AgNO_3$ (0.10 M) as the working, counter, and reference electrodes, respectively. Freshly distilled, degassed CH_2Cl_2 was used as the solvent, with 0.1 M tetra-*n*-butylammonium hexafluorophosphate as the supporting electrolyte.

TOF Transient Photocurrent Measurements for Estimating Charge Mobility. For TOF drift mobility measurements, the sample was prepared on 0.7 mm thick glass substrates coated with indium tin oxide (ITO). Organic film was vacuum deposited onto the patterned ITO, and a 0.1 μm thick aluminum film was deposited by thermal evaporation. The thicknesses were confirmed through scanning electron microscopy (SEM) regarding the cross section of the device after the mobility measurement, which were 3.1, 3.2, 3.3, 3.5, 3.0, and 3.6 μm for ***o*-Cb**, ***m*-Cb**, ***p*-Cb**, ***o*-Bz**, ***m*-Bz**, and ***p*-Bz**, respectively. The ITO side was irradiated with pulsed laser light into the organic film for the generation of photocurrent. The wavelength and pulse width of the laser (Photon Technology International, GL-3300) were 337 nm and 1 ns, respectively.[13] Various bias voltages were applied to the ITO electrode, and a 100 Ω resistor was connected to the aluminum electrode. The opposite side of the resistor was connected to the ground. Also, the photocurrent was measured across the resistor using an oscilloscope.

Calculation Details. All the calculations were performed on the platform of the Gaussian 09 package.[14] The equilibrium structures of neutral singlet and neutral triplet states were obtained from the geometry optimizations performed at the B3LYP/6-31G(D,P) levels of theory, which were confirmed to be global minima by evaluating vibrational frequencies. Most of the single-point energies were calculated at the same level of theory, whereas the calculation of Kohn−Sham energy levels was refined using the B3LYP/6-311+G-(D,P) level of theory. The lowest triplet energies were estimated by calculating ΔSCF, which was obtained by subtracting the SCF energy of the neutral singlet state from that of the triplet state on the basis of optimized geometries.[15] Zero-point vibrational energy (ZPVE) corrections were also taken into account.

OLED Devices. The OLED devices were fabricated on glass substrates precoated with a 150 nm ITO layer having a sheet resistance of 10 Ω/square. The ITO glass was precleaned using a conventional solvent cleaning method. The ITO surface was cleaned again with a UV ozone treatment immediately before depositing the hole transporting layer (HTL). The organic, LiF, and Al layers were deposited sequentially onto the substrate without breaking the vacuum. The current−voltage characteristics of OLEDs were measured using a source measure unit (Keithley 236). The electroluminescence spectra, luminance, and commission internationale de l'elcairage (CIE) coordinates were measured using a spectroradiometer (Photo Research PR650). Assuming Lambertian emission, the external quantum efficiency (EQE) was calculated from the luminance, current density, and electroluminescence spectrum.[16]

RESULTS

Sample Preparation. CzPh-substituted carboranes and benzenes,[8] ***o*-Cb**, ***m*-Cb**, and ***p*-Cb**, and *para*-benzene, ***p*-Bz**,[17,18] were prepared using previously reported methods. ***o*-Bz** and ***m*-Bz** were synthesized by the Suzuki coupling reaction between two equivalents of 4-(carbazol-9-yl) phenylboronic acid and 1,2- or 1,3-dibromobenzene, as shown in Scheme S1 (Supporting Information). All products were isolated by flash column chromatography and further purified by train sublimation in moderate yield. The formation of all compounds was confirmed by high-resolution mass spectrometry and elemental analyses. The compounds showed the expected signals in their ^1H and ^{13}C NMR spectra. Finally, the structural identities of representative examples ***p*-Cb** and ***p*-Bz** were authenticated by means of a single-crystal X-ray crystallography. Later in the following section, a detailed description of the molecular geometry governed by the structural motif either by carborane or benzene is to be made in greater detail.

Photophysical Properties. The absorption (UV) and PL spectra of the carbazoles studied are shown in Figure 1, and

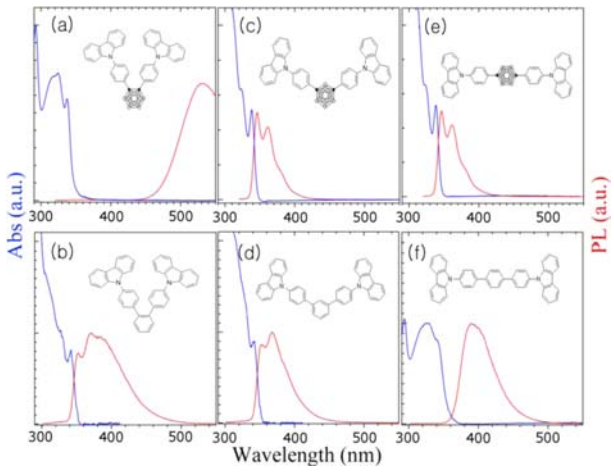

Figure 1. Room-temperature UV/vis absorption and normalized photoluminescence spectra in the solutions of cyclohexane for benzene and carborane based CzPhs.

their steady-state photochemical properties are summarized in Table 1. In particular, there is a stark difference between

Table 1. Optical and Electronic Properties of the Compounds[a]

compounds	abs. λ_{max} [nm]	PL λ_{max} [nm]	Stokes shift [cm^{-1}]	E_g^{opt} (eV)	E_{HOMO} (eV)[b]	E_{LUMO} (eV)[c]
***o*-Cb**	336	-	-	-	−6.02	−2.9[d]
***m*-Cb**	338	346	684	3.63	−6.05	−2.42
***p*-Cb**	338	346	684	3.63	−6.04	−2.41
***o*-Bz**	342	352	831	3.58	−6.04	−2.46
***m*-Bz**	342	352	831	3.58	−6.04	−2.5
***p*-Bz**	342	389	3533	3.43	−6.05	−2.62

[a]The HOMO and LUMO levels were determined using the following equations. [b]E_{HOMO} (eV) = $-e(E_{onset}^{ox} + 4.8)$. [c]E_{LUMO} (eV) = $-e(E_{HOMO} - E_g^{opt})$. [d]E_{LUMO} (eV) = $-e(E_{onset}^{red} + 4.8)$.

dx.doi.org/10.1021/ja3066623 | J. Am. Chem. Soc. 2012, 134, 17982−17990

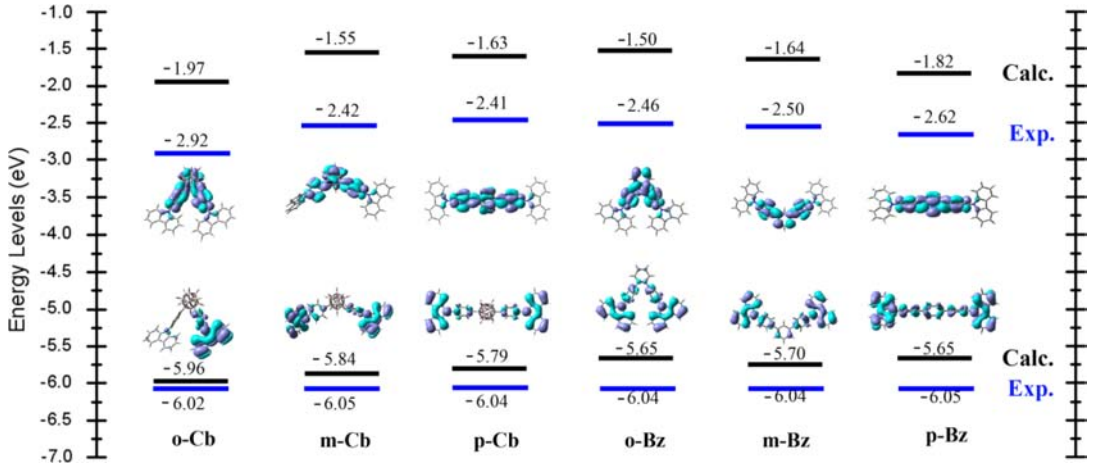

Figure 2. Calculated HOMO/LUMO molecular orbitals and comparison with the experimental energy levels: experimental data are shown in blue, while calculated ones are in black.

carborane and benzene based carbazoles in the PL spectra depending on the geometries; ortho-substitution at the carborane (***o*-Cb**) and para-substitution at the benzene (***p*-Bz**) give rise to effective electronic couplings resulting in a red-shifted PL spectra where the extent of the shift is much more profound for ***o*-Cb**. Also, all benzene-based carbazoles and ***o*-Cb** exhibit featureless emission spectra indicating that there exist electronic couplings between CzPh units interconnected by either benzene or *ortho*-carborane. By contrast, as can be seen in Figure 1c and 1e, for ***m*-Cb** and ***p*-Cb**, notable features are found in UV and PL spectra, which are essentially the same with very small Stokes shifts. This indicates that absorption and emission energy states are originated from the CzPh unit.[19] Furthermore, the characteristic CzPh unit's transverse and parallel transitions are evidently seen at 324 and 338 nm, respectively, in the UV spectra of ***m*-Cb** and ***p*-Cb**. Unlike ***m*-Cb** and ***p*-Cb**, ***o*-Cb** shows a unique photophysical property at room temperature; formation of a new CT energy state is evident in a molecular array of donor−acceptors found in the ***o*-Cb** backbone.[8] This new energy state is due to the special geometry, in which electron donors (CzPhs) are placed on carborane at ortho-substitution sites. Figure 1a shows a red-shifted PL emission supporting for the dyad character of ***o*-Cb**. However, ***o*-Bz**[20] of Figure 1b does not exhibit similar dyad behavior. This in turn manifests the electron-accepting capability of carborane with an emphasis on the geometrical factor; the ortho-substitution creates an energy-accepting state comprising a bond between two carbon atoms of the *o*-carborane. On the basis of the steady-state photophysical properties given by absorption and emission spectra, it can be said that *meta*- and *para*-carboranes do not allow any electronic coupling and simply provide the substitution sites; PL spectra of Figure 1c and 1e show distinct vibronic features of isolated CzPh for both ***m*-Cb** and ***p*-Cb**. From the UV and PL spectra of benzene-based carbazoles (Figure 1b, 1d, and 1f), it is obvious that the benzene platform contributes greatly in electronic couplings, and the para-position is most signified (Figure 1f). Although the meta-position is less affected by electronic coupling among the benzene series, it still exhibits larger electronic coupling when compared with those found in ***m*-Cb** and ***p*-Cb**. Steady-state photophysical data indicate effective excited state energy confinement, from which high T_1 energies for ***m*-Cb** and ***p*-Cb** are expected.

HOMO/LUMO Energy Levels. The highest occupied molecular orbital (HOMO) energy levels of the compounds were determined by CV experiments and are listed in Table 1. All compounds exhibited quasi-reversible oxidation peaks. The HOMO energy levels were estimated from the first oxidation onset potential, exhibiting approximately −6.05 ± 0.03 eV. The lowest unoccupied molecular orbital (LUMO) energy level of ***o*-Cb** was determined from the first reduction onset potential, which is −2.90 eV. The LUMO energy levels of the other compounds were estimated from the optical band gaps and the HOMO energy levels because no cathodic reduction processes were recorded except for ***o*-Cb**. Most of the LUMO energy levels show similar values in the range of −2.45 ± 0.05 eV except for ***o*-Cb** and ***p*-Bz** whose LUMOs are significantly lower than those of the rest shown to be −2.90 and −2.62 eV, respectively. Again, a markedly lowered LUMO clearly explains the electron-accepting capability observed in ***o*-Cb**, which is the unique characteristic of *ortho*-carborane.[8]

Figure 2 illustrates the comparison between the experimental and calculated energy levels, and the calculated physical properties are listed in Table 2. The calculated HOMO levels

Table 2. DFT Calculation Results of HOMO/LUMO Energy Levels, Triplet Energies, and Permanent Dipole Moments

compounds	HOMO[a] (eV)	LUMO[a] (eV)	T_1−S_0 (eV)	dipole Moment (D)
***o*-Cb**	−5.96	−1.97	2.46 (2.34)[b]	4.11
***m*-Cb**	−5.84	−1.55	3.16 (2.98)[b]	1.64
***p*-Cb**	−5.79	−1.63	3.16 (2.97)[b]	0.00
***o*-Bz**	−5.65	−1.50	2.80 (2.68)[b]	2.62
***m*-Bz**	−5.70	−1.64	2.84 (2.72)[b]	1.71
***p*-Bz**	−5.65	−1.82	2.57 (2.53)[b]	0.04

[a]Carried out at the B3LYP/6-311+G(D,P) level of theory. The others were calculated at the B3LYP/6-31G(D,P) level of theory. [b]ZPVE corrected results.

are in the range of −5.86 ± 0.1 eV for the carborane-based compounds and −5.68 ± 0.03 eV for the benzene-based compounds, which are higher than the experimental values of −6.0 eV. The HOMO wave functions are delocalized over two CzPhs for all of the compounds with only one exception for ***o*-Cb**. The molecular orbital distributions of LUMOs are located over central carborane cages and benzenes. The calculated

dx.doi.org/10.1021/ja3066623 | J. Am. Chem. Soc. 2012, 134, 17982−17990

energy levels of LUMOs show higher values than the experimental ones; however, the values are consistently shifted by +0.91 ± 0.12 eV for the six compounds, which is consistent with the reports by Su et al.[4c] This correspondence supports the appropriateness of the calculation. The LUMO levels of the compounds show values comparable to normal carbazole-based materials in the range of −2.50 eV, except for those of ***o*-Cb** and ***p*-Bz**.

The origin of deep LUMO level of ***o*-Cb** (−2.92 eV) is related to the electronic coupling between CzPh and the carborane cage.[8] The relatively deep LUMO level of ***p*-Bz** (−2.62 eV) is comparable to the other electron-transporting materials in the range of −2.7 eV.[4c] This is mainly caused by central triphenyl chromophores, from which electron mobility is also likely to be originated. This will be contemplated in the following mobility description section.

Triplet Energies. The properties of triplet excited states for the compounds were estimated using low-temperature (77 K) time-resolved PL experiments in a dilute solution of 2-methyltetrahydrofuran (MTHF), as shown in Figure 3. After 1 ms

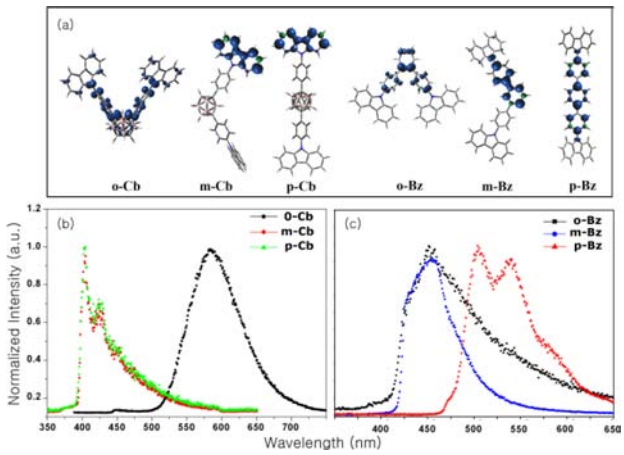

Figure 3. (a) Spin density distributions of carborane and benzene based CzPhs in their first triplet excited states calculated at the UB3LYP/6-31G(D,P) level of theory. Phosphorescence (1 ms delay) spectra of (b) the carborane and (c) the benzene based CzPhs in MTHF at 77 K.

from excitation, most of the fluorescent emissions decayed, and phosphorescent emissions enhanced. The highest energy phosphorescence peak is taken as triplet energy, and the corresponding values are listed in Table 3. T_1 energies of ***o*-Cb** and ***p*-Bz** are in the lower range of 2.5 eV, followed by those of ***o*-Bz** and ***m*-Bz** of 2.74 eV, finally reaching the highest value of 3.05 eV for ***m*-Cb** and ***p*-Cb**. Also, these observed values are closely matched to those calculated (see the values shown in Table 2). Of special importance is a difference in the behavior of triplet wave functions that reside in the molecular arrays formed by benzene and carborane based CzPhs, as illustrated in Figure 3a.

Table 3. Experimentally Determined Physical Properties of the Compounds

compounds	T_1 (eV)[a]	electron mobility ($cm^2/(V\ s)$)[b]	hole mobility ($cm^2/(V\ s)$)[b]	thermal properties $T_g/T_c/T_m$ (°C)[c]
***o*-Cb**	2.12	-	1.97×10^{-4}	130/−/297
***m*-Cb**	3.05	-	6.47×10^{-4}	132/197/286
***p*-Cb**	3.05	-	1.10×10^{-3}	164/−/>400
***o*-Bz**	2.74	-	6.75×10^{-4}	106/−/251
***m*-Bz**	2.74	-	8.35×10^{-4}	121/−/256
***p*-Bz**	2.47	2.5×10^{-4}	1.30×10^{-3}	150/−/325

[a]In MTHF (77 K). [b]Under electric field of 5×10^5 V/cm. [c]Determined by differential scanning calorimetry (DSC).

It is well-known that to acquire high triplet energy the triplet wave functions should be localized.[4a] This criterion is well applied to the compounds of this study in that, except for ***o*-Cb**, the carborane-based CzPhs, ***m*-Cb** and ***p*-Cb**, localize their triplet wave functions to one end of the carbazolyl unit. This again explains the lower triplet energy of ***o*-Cb** in the carborane series and accounts for the anomalous photochemical behavior of ***o*-Cb**. On the other hand, the benzene-based CzPhs, ***o*-Bz**, ***m*-Bz**, and ***p*-Bz**, either locate their triplet wave functions to the central benzenes for ***o*-Bz** or spread them over to the biphenyl for the ***m*-Bz** or triphenyl for the ***p*-Bz** group rather than localize to one end of the carbazolyl unit. This spread of triplet wave functions makes the benzene systems fail to bear a higher T_1 energy. However, the triplet wave functions of meta- and para-substituted carboranes are highly localized to a carbazolyl end-on group bearing a high T_1 of 3.05 eV, as shown in Figure 3a. Also, ***m*-Cb** and ***p*-Cb** show a well-developed T_1 state with the same vibronic coupling pertinent to CzPh,[9] which is obviously shown in Figure 3b.

Thermal Properties. The thermal properties of the compounds were determined by differential scanning calorimetry (DSC) analysis as listed in Table 3. A heating rate of 10 °C min^{-1} was used after the first melting, which was followed by rapid cooling to room temperature. As shown in Figure S3 (Supporting Information), the first heating cycle revealed a T_m, and in subsequent heating cycles, weak endothermic transitions associated with T_g were found. As a result, all of the carborane-based compounds showed high T_g above 130 °C. Moreover, the T_g value of the derivatives increased when changing the position of the substitution groups at the carborane cluster, exhibiting ***o*-Cb** (130 °C) < ***m*-Cb** (132 °C) < ***p*-Cb** (164 °C), as shown in Table 3. In particular, the linear shape of ***p*-Cb** demonstrates a relatively high glass transition temperature, and no distinct crystallization temperature was observed in the range between 30 and 350 °C, which demonstrates stable glasses of this material in its film state.

For comparison, we also examined benzene-based compounds and found relatively low glass transition temperatures in which ***o*-Bz**, ***m*-Bz**, and ***p*-Bz** show T_g values of 106, 121, and 150 °C, respectively. From this result, the restricted motion[20] and higher molecular mass nature[21] of the carborane cluster are thought to contribute a great deal to the increased T_g values. Granting that higher T_g hosts can contribute device stability for PHOLEDs, and the carborane hosts developed in this study, ***m*-Cb** or ***p*-Cb**, can shed new light on device stability and lifetime.[22]

Crystal Packing from X-ray Crystallography. A crystal structure could provide important information on the thermal property of the solid state as well as on charge mobility. The crystals of ***p*-Cb** and ***p*-Bz** were grown from a CH_2Cl_2/hexane mixed solution. Their crystal data and collection parameters are summarized in Tables S1 and S2 (Supporting Information). Although the photophysical characteristics of ***p*-Bz** have been reported as a bipolar host,[17,18] its structure has never been established. For this reason, this work includes a structural study of ***p*-Bz** along with that of ***p*-Cb** for comparison. ***p*-Cb** and

dx.doi.org/10.1021/ja3066623 | J. Am. Chem. Soc. 2012, 134, 17982−17990

p-**Bz** crystallize in the *P*bca and $P2_1/n$ space group, respectively (Figure 4). With regards to the crystal structure of *p*-**Cb**, a half

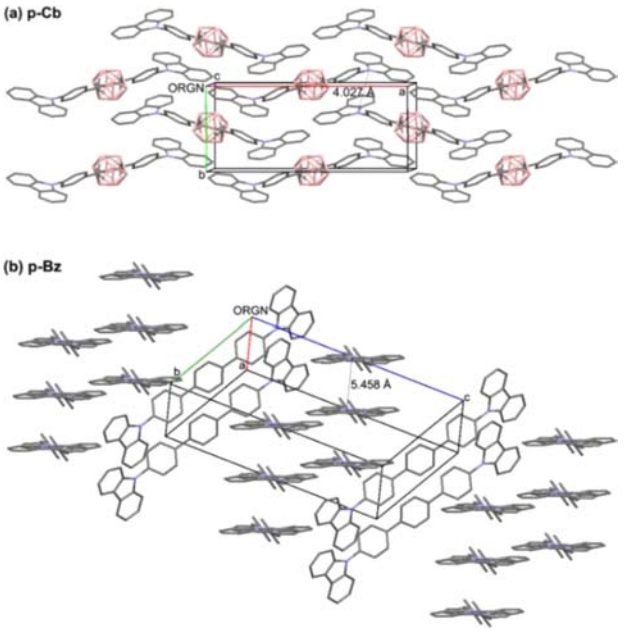

Figure 4. Molecular packings of (a) *p*-**Cb** and (b) *p*-**Bz** with unit cell by the Mercury program. Hydrogen atoms are omitted for clarity.

molecule belongs to an asymmetric unit, and a molecule is completed by another half molecule translated by an inversion symmetry located at the center of the carborane cage [symmetry code: $1 - x$, $1 - y$, $1 - z$]. Similarly a complete molecule of *p*-**Bz** is accomplished through an inversion center located at the centroid of the benzene ring $C_{cent}\cdots C_{cent}$ [symmetry code: $-x$, $-y$, $-z$]. Thus, for each structure, there are two molecules in a unit cell.

Molecular packings of *p*-**Cb** and *p*-**Bz** are shown in Figure 4a and 4b, respectively. The aromatic groups and carbazole units of the structure have a dominating influence upon the overall crystal packing. The crystal structures for both *p*-**Cb** and *p*-**Bz** are similar to each other in terms of the overall morphology caused by the inversion symmetry existing at the center of each molecule, whereas the packing motif of *p*-**Cb** is quite different from that of *p*-**Bz**. The undulating topology of the former is highlighted in Figure 4a. The carbazole units of adjacent rows partially overlap between each phenyl ring of carbazole units. However, *p*-**Bz** packs into two different column structures in the *ab* and *bc* planes, respectively, so that the column structures join in a crossing manner with each other at roughly 90° when viewed along the *c*-axis (see Figure 4b and 5b). The N···N distances of *p*-**Cb** and *p*-**Bz** between the overlapped carbazole units are 4.03 and 5.46 Å, respectively. The dihedral angle between the carbazole/phenylene linker of *p*-**Cb** is 16.42°, and the dihedral angles between the carbazole/phenylene linker and the phenylene linker/central phenyl unit of *p*-**Bz** are calculated as 54.08 (6) and 30.6 (2)°, respectively. The shortest C···C distance between the adjacent carbazole units of *p*-**Cb** is 3.36 Å (C17···C14^{i} [symmetry code: (i) $-x + 0.5$, $y + 0.5$, z]), whereas that of *p*-**Bz** is 3.43 Å (C4···C8^{i} [symmetry code: (i) $x + 1$, y, z]), taking into account the van der Waals radii of C being 1.70 Å.[23]

As shown in Figure 5a, the carborane cluster induces favorable packings in the solid-state structure. *p*-**Cb** molecules

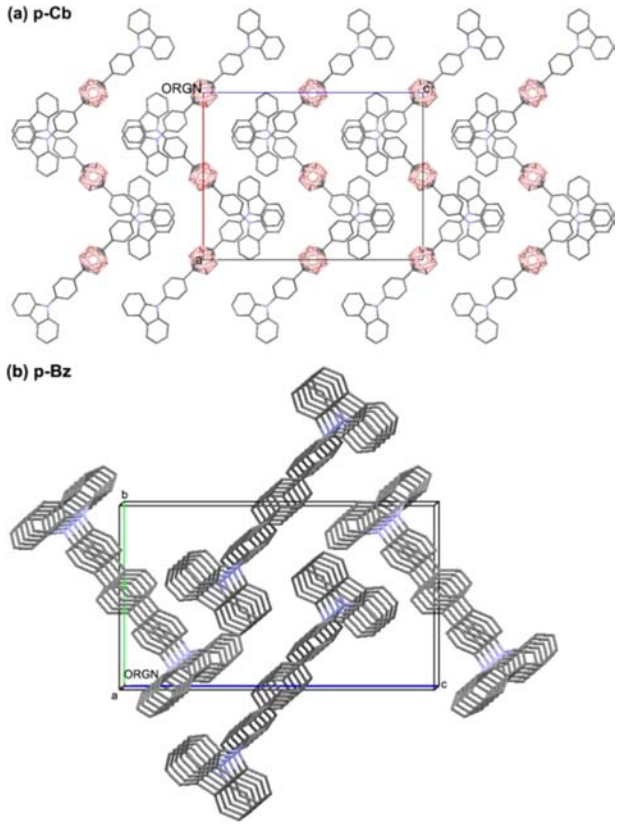

Figure 5. Molecular packings of (a) *p*-**Cb** in the *b*-axis and (b) *p*-**Bz** in the *a*-axis in a single unit cell by the Mercury program. Hydrogen atoms are omitted for clarity.

pack into a zig-zag structure in the *a*-axis. The adjacent carbazole rings are situated in an overlapping mode along the *b*-axis, and the overlapping area is approximately one benzene ring. As shown in Figure 5b, however, *p*-**Bz** packs into a column structure along the *a*-axis and adopts face-to-face packing. All of the adjacent *p*-**Bz** slightly slips along a direction. Although there seems to be no clear measure to estimate the intermolecular interactions for *p*-**Cb** and *p*-**Bz**, based on the interatomic distances between the molecular layers and the orientations in the molecular packings governed by their morphologies, the higher thermal stability of the thin film of *p*-**Cb** is expected.

Charge-Transporting Properties. The charge-transporting properties of the compounds were systematically investigated using TOF transient photocurrent measurements. Figure 6 shows the electric field dependence of the hole and

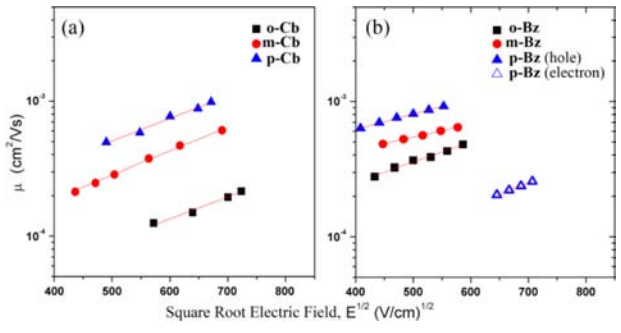

Figure 6. Charge mobility of solid state thin films of (a) carborane and (b) benzene based CzPhs as a function of square root electric field.

dx.doi.org/10.1021/ja3066623 | *J. Am. Chem. Soc.* 2012, 134, 17982−17990

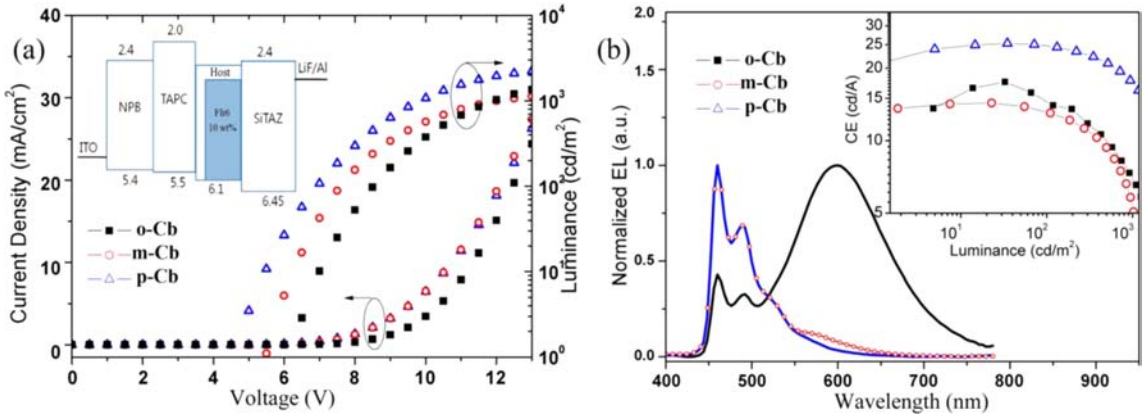

Figure 7. Device characteristics of the PHOLEDs using carborane-based compounds as hosts in the devices with the device structures of ITO/NPB (40 nm)/TAPC (15 nm)/**Host** (10 nm)/**Host**: FIr6 10 wt % (35 nm)/SiTAZ (40 nm)/LiF (0.5 nm)/Al (60 nm). (a) Current–voltage and luminance–voltage curves. Inset: Schematic energy levels of the materials used in the devices. (b) Electroluminescence spectra measured during device operation with a constant current of 1 mA/cm^2. Inset: Current efficiency–luminance curves.

electron mobility for the compounds. All of the mobility data could be well fitted with the Poole–Frenkel function of $\mu = \mu_o \exp(E^{1/2}/\sigma)$, of which the results are summarized in the Supporting Information. Electron mobility was observed only for ***p*-Bz**, and the value is much inferior to that of hole for the same compound. This is a commonly observed phenomenon for benzene-based materials when compared to heteroaromatic-based materials regarding electron-transporting properties.[4c]

Regardless of the benzene or carborane platform, hole mobility appears to be governed by the general geometric rule, in which meta- and para-geometries showed enhanced mobility over the ortho geometry, and among the meta- and para-geometries, the para-isomer proceeds to the meta-isomer in a small degree: ***p*-Cb** and ***p*-Bz** exhibited relatively higher hole mobility among the series. Inferior hole mobility can be related to the geometrical hindrance imposed by two facing bulky π-groups, which would then confuse the intermolecular interactions within the solid-state organization. This confusion would be the greatest in the ortho-isomer and alleviated for meta-isomers. With the same argument, a higher degree of symmetry imposed on the para-geometry can help to increase intermolecular electronic interactions enhancing the charge mobility.[24] The solid-state packing structure for ***p*-Bz** and ***p*-Cb** shown in Figures 4 and 5 provides grounds for such speculation. Taking into account the geometrical preference of para-isomers, ***p*-Cb** and ***p*-Bz** mark the best hole mobility of 1.10×10^{-3} and 1.30×10^{-3} cm^2/(V s), respectively, under an electric field of 5×10^5 cm/V, which is a bias condition similar to that applied for the real device operation.

Device Characteristics. From the structure–property relationships, ***m*-Cb** and ***p*-Cb** are expected to be promising host materials for deep blue PHOLEDs because of their high hole mobility, high thermal stability, and high triplet energy, whereas ***o*-Cb** is expected to exhibit poor performance if it is used as a host for a deep blue guest due to its low triplet energy of 2.36 eV and relatively lower hole mobility compared to the other two. To examine the feasibility of application for carborane-based materials regarding deep blue PHOLEDs, a series of iridium(III)[bis(4,6-difluorophenyl)pyridinato-*N*,$C^{2'}$]-tetrakis(1-pyrazolyl)borate (FIr6) based PHOLEDs were fabricated with the following device structure: ITO/NPB (40 nm)/TAPC (15 nm)/**Host** (10 nm)/**Host**: FIr6 (35 nm, 10 wt %)/SiTAZ (40 nm)/LiF (0.5 nm)/Al (60 nm). Three different host materials were used in three different devices, device A, B, and C, where the **Hosts** are ***o*-Cb**, ***m*-Cb**, and ***p*-Cb**, respectively. A thin interlayer of 1-bis[4-[*N*,*N*-di(4-tolyl)-amino]phenyl]-cyclohexane (TAPC) was inserted between the *N*,*N*′-bis(naphthalen-1-yl)-*N*,*N*′-bis(phenyl)-benzidine (NPB) and EML as a triplet exciton blocking layer since TAPC has a high triplet energy ($T_1 \sim 2.9$ eV). As a deep blue emitter, FIr6 was chosen because it has high PL quantum yield and is commercially available. The electron-transporting layer (ETL) material, bis(4-(4,5-diphenyl-4*H*-1,2,4-triazol-3-yl)-phenyl)-dimethylsilane (SiTAZ), was used for its high triplet energy (2.84 eV), deep HOMO level (6.45 eV), and high LUMO level (2.5 eV).[16b] Figure 7a shows both the current density–voltage and luminance–voltage characteristics. As anticipated from the hole mobility results, the devices using ***m*-Cb** and ***p*-Cb** (device B and C) as hosts show higher current density than device A.

Figure 7b illustrates the current efficiency–luminance curves and normalized EL spectra at a current density of 1 mA/cm^2. Maximum current efficiencies of device A and B are 17.5 and 14.3 cd/A, respectively. These values are quite low compared to the recent reports of deep blue devices.[16] The low efficiency of device A has been expected because of its low triplet energy and CT-type excited states of ***o*-Cb**, which is also observed in the EL spectrum as broad emission ranging from 500 to 750 nm.[8] However, the low efficiency of device B denies easy interpretation considering the high triplet energy and wide band gap of ***m*-Cb**. An abnormal additional peak near 580 nm appears in the EL spectrum of device B, which is different from the FIr6 emission. This peak can be assigned as an electromer emission from the TAPC layer.[25a] This observation implies that parts of the electrons passed through EML without recombination with the holes and reached the TAPC layer, forming an electromer with holes inside the TAPC layer.[25b] Late activation of device A and B (5.5 and 6.3 V) compared to that of device C (4.7 V) can also be attributed to the above inefficient recombination of holes and electrons inside EML. One of the possible reasons for the inefficient recombination of electrons and holes inside EML with host ***m*-Cb** or ***o*-Cb** can be attributed to the interface effects such as slight vacuum level shifts between organic layers, which is in a close relationship with the dipole moment of a molecule.[26,27] Looking at the calculation results in Table 2, dipole moments of ***o*-Cb** and ***m*-**

dx.doi.org/10.1021/ja3066623 | J. Am. Chem. Soc. 2012, 134, 17982–17990

Cb are considerably high compared to that of ***p*-Cb**, which is almost zero.

On the contrary, high current efficiency of 25.3 cd/A (EQE of 15.3%) is achieved for device C, which is comparable to the best results of the FIr6-based monopolar EML devices reported.[16] No additional emission other than FIr6 is seen in the EL spectrum, indicating efficient energy transfer from host to guest and efficient triplet energy confinement into EML. As a result, CIE coordinates of (0.15, 0.24) are obtained at a current density of 1 mA/cm^2. In the case of device B, due to electromer emission, CIE coordinates are shifted to (0.17, 0.25). CIE coordinates of device A exhibit (0.43, 0.41), which show a yellowish white color owing to the long wavelength emission of CT excited states.[8]

DISCUSSION

It is now clear that carborane platforms provide the best synergistic molecular arrays in regards to the blue materials for OLEDs, and among the candidates, ***m*-Cb** and ***p*-Cb** are shown to be the most promising. So far, ***m*-Cb** and ***p*-Cb** confine triplet wave functions effectively to a carbazolyl unit giving rise to the high T_1 which is characteristic of the isolated CzPh chromophore. Moreover, high hole mobility was observed for ***p*-Cb**, which is comparable to that of ***p*-Bz**. In the case of ***p*-Bz**, high hole mobility can be attributed to the extended conjugation due to delocalization of the HOMO wave function and the extensive intermolecular overlap of wave functions.[28] However, this in turn resulted in lower triplet energy due to conjugation. On the contrary, ***p*-Cb** not only shows unperturbed T_1 but also exhibits comparable hole mobility. A symmetric molecular structural motif as well as para-substitution is expected to be the prime reason for the enhanced mobility. From the solid state packing analysis, ***p*-Cb** provided the grounds for such surmises.

Above all, those carborane-based organic materials are quite different from their organic congeners, benzenes, and are even superior to those developed from Si-based organic materials, which disconnect effectively conjugation of the chromophores bridged by the Si atom. As shown in Figure 8, despite the successful energy confinement by the silicon atom, the corresponding silicon template lacks thermal stability, showing a relatively low T_g value of 99 °C. **p-Cb**'s high T_g value has reached the highest among the phosphorescence host materials developed thus far. Considering the fact that the wide band gap host materials for deep blue PHOLEDs developed in our group as well as others are limited only to Si-templates or phosphine oxides,[15] the carborane templates developed in this study provide new insight into designing materials for PHOLEDs. Most of all, the representative example given by the ***p*-Cb** exhibits the most favorable material specifications: a high T_1, high T_g, and good hole mobility.

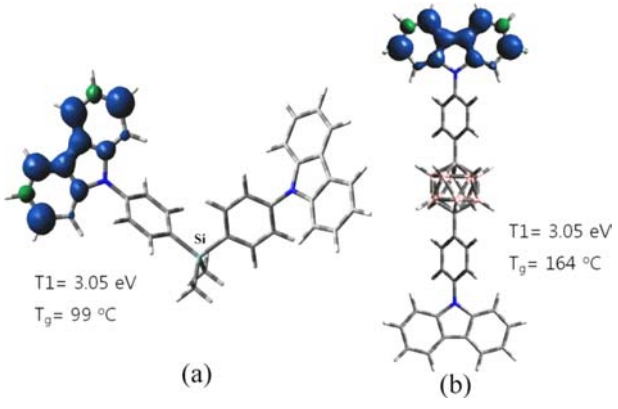

Figure 8. Spin density distribution of (a) Si and (b) carborane-based carbazoles in their first triplet excited states calculated at the UB3LYP/6-31G(D,P) level of theory.

CONCLUSIONS

Three isomeric carborane-based materials (***o*-Cb**, ***m*-Cb**, and ***p*-Cb**) as well as three respective benzene analogues (***o*-Bz**, ***m*-Bz**, and ***p*-Bz**) were synthesized, and their photophysical properties were systematically compared with each other to reveal that the carborane linkers, *m*- and *p*-carboranes, were effective in localizing triplet energy at one end of the CzPh unit reaching their T_1 values of 3.1 eV. Spin density distribution in the first triplet exited state corroborated well to this higher T_1. As we anticipated, a desired higher T_g of 164 °C was recorded for ***p*-Cb**. Comparable hole mobility equivalent to ***p*-Bz** merits the use of inorganic templates, carboranes. In the case of ***p*-Cb**, high triplet energy, high T_g, and high charge mobility were accomplished, which have been regarded as conflicting targets to achieve. Moreover, ***p*-Cb** showed excellent device performance when it was used as a host in EML for deep blue PHOLEDs, exhibiting a high external quantum efficiency of 15.3% and CIE coordinates of (0.15, 0.24), which are comparable to the best results with the simplest device structure. Considering the physical property of ***p*-Cb** and its possibility toward the application regarding real electronic devices, the para-linkage of functional chromophores to a carborane cage is a promising novel strategy for the synthesis of electronic materials.

ASSOCIATED CONTENT

Supporting Information

DSC thermograms and complete listing of the crystal data for ***p*-Bz**, including complete drawings with labeling schemes, bond lengths, and angles. Raw data of TOF measurements for charge mobility are also provided. This material is available free of charge via the Internet at http://pubs.acs.org.

AUTHOR INFORMATION

Corresponding Author

andrew2@korea.ac.kr; sangok@korea.ac.kr

Notes

The authors declare no competing financial interest.

ACKNOWLEDGMENTS

This work is supported by the Basic Science Research Program (No. 2012-0006248) and WCU program (No. R-31-2009-000-10083-0) through the National Research Foundation of Korea (NRF) funded by the Ministry of Education, Science and Technology.

REFERENCES

(1) (a) Zhigang, Li Hong, Meng, *Organic Light-Emitting Materials and Devices*; CRC Press: Boca Raton, FL, 2007. (b) Murphy, A. R.; Frechet, J. M. J. *Chem. Rev.* **2007**, *107*, 1066. (c) Hains, A. W.; Liang, Z.; Woodhouse, M. A.; Gregg, B. A. *Chem. Rev.* **2010**, *110*, 6689.

(2) Xiao, L.; Chen, Z.; Qu, B.; Luo, J.; Kong, S.; Gong, Q.; Kido, J. *Adv. Mater.* **2011**, *23*, 926.

(3) Wu, M. F.; Yeh, S. J.; Chen, C. T.; Murayama, H.; Tsuboi, T.; Li, W. S.; Chao, I.; Liu, S. W.; Wang, J. K. *Adv. Funct. Mater.* **2007**, *17*, 1887.
(4) (a) Avilov, I.; Marsal, P.; Bredas, J.-L.; Beljonne, D. *Adv. Mater.* **2004**, *16*, 1624. (b) Su, S.-J.; Sasabe, H.; Takeda, T.; Kido, J. *Chem. Mater.* **2008**, *20*, 1691. (c) Su, S.-J.; Cai, C.; Kido, J. *Chem. Mater.* **2011**, *23*, 274.
(5) (a) Pohl, A.; Bredas, J. L. *Int. J. Quantum Chem.* **1997**, *63*, 437. (b) Malliaras, G. G.; Herrema, J. K.; Wildeman, J.; Wieringa, H.; Gill, R. E.; Lampoura, S. S.; Hadziioannou, G. *Adv. Mater.* **1993**, *5*, 721. (c) Hilberer, A.; Wildeman, J.; Brouwer, H.-J.; Garten, F.; Hadziioannou, G. *SPIE Proc.* **1995**, *2528*, 74.
(6) (a) Grimes, R. N. *Carboranes*, 2nd ed.; Acadamic Press: New York, Mar-2011. (b) Bregadze, V. I. *Chem. Rev.* **1992**, *92*, 209. (c) Schwab, P. F. H.; Levin, M. D.; Michl, J. *Chem. Rev.* **1999**, *99*, 1863. (d) Ko, J.; Kang, S. O. *Adv. Organomet. Chem.* **2001**, *47*, 61.
(7) (a) Colquhoun, H. M.; Herbertson, P. L.; Wade, K.; Baxter, I.; Williams, D. J. *Macromolecules* **1998**, *31*, 1694. (b) Schoberl, U.; Magnera, T. F.; Harrison, R. M.; Fleischer, F.; Pflug, J. L.; Schwab, P. F. H.; Meng, X.; Lipiak, D.; Noll, B. C.; Allured, V. S.; Rudalevige, T.; Lee, S.; Michl, J. *J. Am. Chem. Soc.* **1997**, *119*, 3907. (c) Peterson, J. J.; Werre, M.; Simon, Y. C.; Coughlin, E. B.; Carter, K. R. *Macromolecules* **2009**, *42*, 8594.
(8) (a) Wee, K.-R.; Han, W.-S.; Cho, D. W.; Kwon, S.; Pac, C.; Kang, S. O. *Angew. Chem., Int. Ed.* **2012**, *51*, 2677. (b) Kokado, K.; Chujo, Y. *J. Org. Chem.* **2011**, *76*, 316. (c) Peterson, J. J.; Davis, A. R.; Werre, M.; Coughlin, E. B.; Carter, K. R. *ACS Appl. Mater. Interfaces* **2011**, *3*, 1796.
(9) Han, W.-S.; Son, H.-J.; Wee, K.-R.; Min, K.-T.; Kwon, S.; Suh, I.-H.; Choi, S.-H.; Jung, D.-H.; Kang, S. O. *J. Phys. Chem. C* **2009**, *113*, 19686.
(10) Ge, Z.; Hayakawa, T.; Ando, S.; Ueda, M.; Akiike, T.; Miyamoto, H.; Kajita, T.; Kakimoto, M.-a. *Chem. Lett.* **2008**, *37*, 262.
(11) *SMART and SAINT*; Bruker Analytical X-Ray Division: Madison,WI, 2002.
(12) Sheldrick, G. M. *SHELXTL-PLUS Software Package*; Bruker Analytical X-Ray Division: Madison, WI, 2002.
(13) Wee, K.-R.; Han, W.-S.; Son, H.-J.; Kang, S. O.; Kwon, S. *Rev. Sci. Instrum.* **2009**, *80*, 096106.
(14) Frisch, M. J.; Trucks, G. W.; Schlegel, H. B. et al., *GAUSSIAN 09*, revision B.01; Gaussian, Inc.: Wallingford, CT, 2010. Complete citation is provided in ref 3 in the Supporting Information.
(15) (a) Kim, D.; Salman, S.; Coropceanu, V.; Salomon, E.; Padmaperuma, A. B.; Sapochak, L. S.; Kahn, A.; Brédas, J.-L. *Chem. Mater.* **2010**, *22*, 247. (b) Padmaperuma, A. B; Sapochak, L. S.; Burrows, P. E. *Chem. Mater.* **2006**, *18*, 2389.
(16) (a) Fukagawa, H.; Watanabe, K.; Tsuzuki, T.; Tokito, S. *Appl. Phys. Lett.* **2008**, *93*, 133312. (b) Kwon, S.; Wee, K.-R.; Kim, A.-L.; Kang, S. O. *J. Phys. Chem. Lett.* **2010**, *1*, 295. (c) Wee, K.-R.; Kim, A.-L.; Jeong, S.-Y.; Kwon, S.; Kang, S. O. *Org. Electron.* **2011**, *12*, 1973.
(17) Jeon, J. Y.; Park, T. J.; Jeon, W. S.; Park, J. J.; Jang, J.; Kwon, J. H.; Lee, J. Y. *Chem. Lett.* **2007**, *36*, 1156.
(18) Park, T. J.; Jeon, W. S.; Park, J. J.; Kim, S. Y.; Lee, Y. K.; Jang, J.; Kwon, J. H. *Thin Solid Films* **2008**, *517*, 896.
(19) (a) Platt, J. R. *J. Chem. Phys.* **1949**, *17*, 484. (b) Johnson, G. E. *J. Phys. Chem.* **1974**, *78*, 1512.
(20) (a) Salbeck, J.; Yu, N.; Bauer, J.; Weissörtel, F.; Bestgen, H. *Synth. Met.* **1997**, *91*, 209. (b) Weinfurtner, K. H.; Weissörtel, F.; Harmgarth, G.; Salbeck, J *Proc. SPIE-Int. Soc. Opt. Eng.* **1998**, *3476*, 40.
(21) (a) Naito, K.; Miura, A. *J. Phys. Chem.* **1993**, *97*, 6240. (b) Naito, K. *Chem. Mater.* **1994**, *6*, 2343.
(22) (a) Tokito, S.; Tanaka, H.; Taga, Y. *Appl. Phys. Lett.* **1996**, *69*, 878. (b) Tokito, S.; Noda, K.; Fujikawa, H.; Taga, Y.; Kimura, M.; Shimada, K.; Sawaki, Y. *Appl. Phys. Lett.* **1996**, *77*, 160.
(23) Li, Y. -X; Chen, Z.; Cui, Y.; Xia, G. −M.; Yang, X.-F. *J. Phys. Chem. C* **2012**, *116*, 6401.
(24) Yokoyama, D.; Sasabe, H.; Furukawa, Y.; Adachi, C.; Kido, J. *Adv. Funct. Mater.* **2011**, *21*, 1375.
(25) (a) Kalinowski, J.; Giro, G.; Cocchi, M.; Fattori, V.; Marco, P. *Appl. Phys. Lett.* **2000**, *76*, 2352. (b) Kwon, S.; Wee, K.-R.; Pac, J.; Kang, S. O. *Org. Electron.* **2012**, *13*, 645.
(26) (a) Rajagopal, A.; Wu, C. I.; Kahn, A. *J. Appl. Phys.* **1998**, *83*, 2649. (b) Kera, S.; Yabuuchi, Y.; Yamane, H.; Setoyama, H.; Okudaira, K. K.; Kahn, A.; Ueno, N. *Phys. Rev. B* **2004**, *70*, 085304.
(27) Xin, Q.; Duhm, S.; Hosoumi, S.; Ueno, N.; Tao, X.-t.; Kera, S. *J. Phys. Chem. C* **2011**, *115*, 15502.
(28) (a) Su, S.-J.; Takahashi, Y.; Chiba, T.; Takeda, T.; Kido, J. *Adv. Funct. Mater.* **2009**, *19*, 1260. (b) Coropceanu, V.; Cornil, J.; Filho, D. A.; Oliver, Y.; Silbey, R.; Bredas, J. L. *Chem. Rev.* **2007**, *107*, 926.